Neutron spectroscopy studies of the crystal-field interaction in RET_4Al_8 compounds (RE=Tb, Ho or Er; T=Mn, Fe or Cu)

1995 J. Phys.: Condens. Matter 7 7981

(http://iopscience.iop.org/0953-8984/7/41/007)

J. Phys.: Condens. Matter 7 (1995) 7981–7989. Printed in the UK

Neutron spectroscopy studies of the crystal-field interaction in RET_4Al_8 compounds (RE = Tb, Ho or Er; T = Mn, Fe or Cu)

R Caciuffo†, G Amoretti‡, K H J Buschow§, O Moze‡, A P Murani‖ and B Paci†

† Dipartimento di Scienze dei Materiali e della Terra, Sezione Fisica, Università di Ancona, Via Brecce Bianche, 60131-Ancona, Italy

‡ Dipartimento di Fisica, Università di Parma, Viale delle Scienze, 43100-Parma, Italy

§ van der Waals–Zeeman Laboratorium, Universiteit van Amsterdam, Valckenierst. 65, 1018 XE, Amsterdam, The Netherlands

‖ Institut Laue–Langevin, 156-X, F-38042 Grenoble Cédex, France

Received 24 March 1995, in final form 26 June 1995

Abstract. Inelastic neutron scattering experiments have been performed on some members of the tetragonal RET_4Al_8 series of compounds (RE = Tb, Ho or Er; T = Mn, Fe or Cu) in order to determine the crystal-field potential at the RE site. A consistent set of the crystal-field parameters has been obtained from the experimental data by a least-squares fit procedure, using information on the second-order term deduced from Mössbauer spectroscopy measurements in $^{155}GdT_4Al_8$. The results obtained have been used to estimate the rare-earth contribution to the magnetic anisotropy constants and to discuss the characteristics of possible spin reorientation processes.

1. Introduction

The search for novel starting materials for permanent magnet applications has been centred for some time on ternary systems of the type RE–T–M or RE–T–T (RE = rare earth; T = transition metal; M = metalloid), and a large number of new phases exhibiting different stoichiometries and a variety of magnetic properties have been synthesized [1]. Among these systems, the $RE(T,M)_{12}$ series (T = Fe, Mn, Cr or Ni; M = Ti, V, Mo, W, Re or Si), crystallizing in the tetragonal $ThMn_{12}$ type of structure has attracted considerable interest because of the high Fe to RE ratio [2–4]. In these compounds the transition-metal sublattice prefers an easy-magnetization direction along the crystallographic c axis and favours uniaxial magnetic anisotropy. On the other hand, the anisotropy of the rare-earth sublattice is mainly a consequence of the interaction between the electrostatic field of the ions surrounding the RE site and the asymmetric charge cloud of the 4f electrons. The signs of the RE anisotropy constants are thus determined by the signs and the relative magnitude of the crystal-field parameters (CF) B_n^m, and both easy-plane and easy-axis magnetic arrangements of the RE sublattice are possible, with the easy-plane configurations generally exhibited by those REs with negative second-order Stevens factors [5]. In these latter cases, because of the different temperature dependences of the RE and T sublattice anisotropies, spin reorientation transitions or anomalous magnetic processes are observed.

0953-8984/95/417981+09$19.50

Knowledge of the CF potential acting at the RE sites is therefore of great importance in explaining almost all the magnetic properties of $RET_{12-x}M_x$ compounds. For this reason, in order to determine the parameters B_n^m of the CF Hamiltonian, we have performed a number of inelastic neutron scattering (INS) experiments on some members of the RET_4Al_8 family (RE = Tb, Ho or Er; T = Mn, Fe or Cu). The compounds investigated were chosen because they have a rather weak exchange interaction and remain paramagnetic down to low temperatures [6, 7]. The single-ion electronic excitations can then be directly observed by neutron spectroscopy without the complications that a strong molecular field would imply.

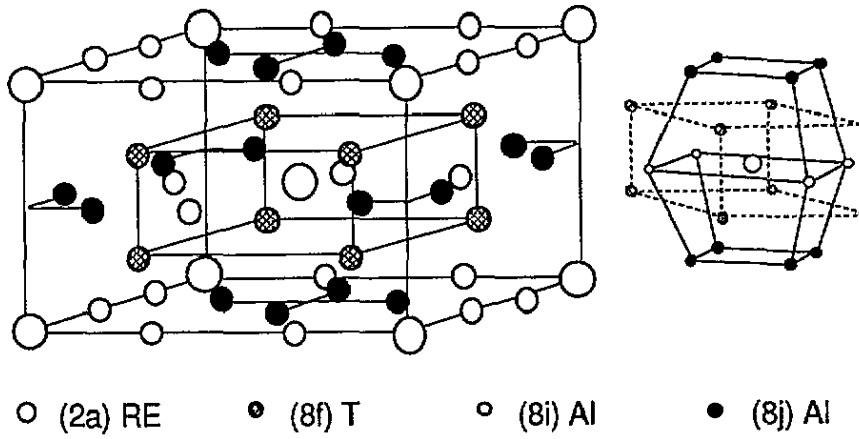

Figure 1. The tetragonal crystal structure of RET_4Al_8 compounds (space group, $I4/mmm$), and the coordination polyhedron around the RE sites.

The $ThMn_{12}$ crystallographic structure, shown in figure 1, is body centred tetragonal, with space group $I4/mmm$, and two formula units per unit cell [8]. The RE atoms occupy the 2a sites of point symmetry $4/mmm$ at the corners and the centres of tetragonal prisms. They are surrounded by four Al atoms at about 3.0 Å (8i sites), by eight Al at 3.2 Å (8j sites) and by eight transition-metal atoms located at the 8f sites at 3.4 Å. Neutron diffraction experiments on RET_4Al_8 revealed only small deviations from the ideal site occupations and a strong preferential site occupancy [9].

In $ErCu_4Al_8$, an antiferromagnetic order develops at $T_N = 6$ K. Magnetic susceptibility and Mössbauer spectroscopy data clearly indicate that the Cu sublattice is non-magnetic and that only the Er ions contribute to the effective paramagnetic moment ($\mu_{eff} = 9.6\mu_B$) [6]. On the other hand, two magnetic transitions are exhibited by $ErFe_4Al_8$, with the Er sublattice ordering at 25 K and the Fe sublattice at 111 K. The iron paramagnetic effective moment deduced from the susceptibility curves is $4.3(2)\mu_B$ per Fe ion [6]. Neutron diffraction experiments show that Er orders antiferromagnetically with a ferromagnetic component and a helical component incommensurate with the lattice, whilst the Fe sublattice has both ferromagnetic and antiferromagnetic components [10]. A neutron diffraction study of $REFe_4Al_8$ (RE = Er, Ho or Dy) suggests a spin-glass behaviour of the RE sublattice below $T_{SG} = 180$ K, coexistent at lower temperatures with a long-range antiferromagnetic order of the Fe sublattice [11]. Frustration has been attributed to the RKKY exchange coupling of the RE and Fe moments. A similar behaviour has been reported also for the isostructural actinide compounds $AnFe_4Al_8$ (An = Th, U or Np) [12]. In $REMn_4Al_8$ (RE = Er, Ho or Tb), susceptibility measurements show one magnetic transition only, and Mössbauer spectroscopy experiments indicate that the Mn ions develop long-range

magnetic order under the influence of the ordering of the RE sublattice [6]. The details of the magnetic structure in the ordered phases is not yet known. Preliminary neutron diffraction measurements on $TbMn_4Al_8$ ($T_N = 21$ K) were not able to detect long-range magnetic order down to 2 K. Further low-temperature neutron diffraction measurements are being performed in order to clarify and assess this point. The crystallographic parameters and the transition temperatures for the compounds investigated in the present study are reported in table 1.

Table 1. Lattice parameters and magnetic ordering temperatures for the RET_4Al_8 compounds investigated [6, 9].

	$TbMn_4Al_8$	$HoMn_4Al_8$	$ErMn_4Al_8$	$ErCu_4Al_8$	$ErFe_4Al_8$
a (Å)	8.8680(2)	8.8503(2)	8.8290(2)	8.7120(2)	8.7040(2)
c (Å)	5.1029(2)	5.0968(2)	5.0960(2)	5.1300(2)	5.0370(2)
T_N (K)	21(2)	14(2)	15(2)	6(1)	25(2), 111(2)

Preliminary INS results on $REMn_4Al_8$ (RE = Er, Ho or Tb) have already been reported [13, 14]. In this paper, these data and the results of further measurements on $ErFe_4Al_8$ and $ErCu_4Al_8$ are analysed in a consistent manner to obtain a realistic set of CF parameters for the RE ions in the $ThMn_{12}$ type of structure.

2. Experimental details and results

All the investigated samples ($TbMn_4Al_8$, $HoMn_4Al_8$, $ErMn_4Al_8$, $ErFe_4Al_8$ and $ErCu_4Al_8$) were prepared in the polycrystalline form by melting stoichiometric amounts of the elements (of at least 99.9% purity) in an arc furnace under a reduced argon atmosphere. Selected specimens of each sample were subsequently characterized by x-ray diffraction and were shown to be single phase with all Bragg peaks consistent with the $ThMn_{12}$ structure. Room-temperature neutron diffraction data were previously used to refine atomic coordinates and site populations in the tetragonal unit cell. The results showed small deviations from the ideal site occupation, with about 5% of the T atoms going into the 8j site and about 2% of them going into the 8i site [9].

About 40 g of each compound were mounted in an aluminium can onto a liquid-He cryostat for the INS experiments. Measurements on $ErMn_4Al_8$ were performed using the direct geometry time-of-flight chopper spectrometer HET of the ISIS facility at RAL (incident energy $E_i = 40$ meV, scattering angle range from 5 to 136° and energy resolution at the elastic peak of about 0.6 meV). INS experiments on $TbMn_4Al_8$ and $HoMn_4Al_8$ were performed on the time-focused crystal analyser spectrometer TFXA at ISIS (final energy $E_f = 4$ meV, scattering angle $\phi = 133°$ and neutron energy transfer resolution smaller than 5% in the investigated range). A sample of non-magnetic YMn_4Al_8 was used in order to identify contributions to the neutron spectra arising from vibrational scattering. The neutron scattering functions for $ErCu_4Al_8$ and $ErFe_4Al_8$ were measured on the direct-geometry time-of-flight spectrometer IN4 at the Institut Laue–Langevin in Grenoble, France (incident energy of 17 meV, scattering angles ϕ between 10 and 74° and energy transfer resolution smaller than 6%).

The dependences on the energy transfer $\hbar\omega$ of the neutron scattering function $S(\phi, \hbar\omega)$ obtained at a temperature $T = 58$ K for $TbMn_4Al_8$ and $HoMn_4Al_8$ are shown in figure 2. The measurements are performed at constant scattering angle and the scattering vector Q

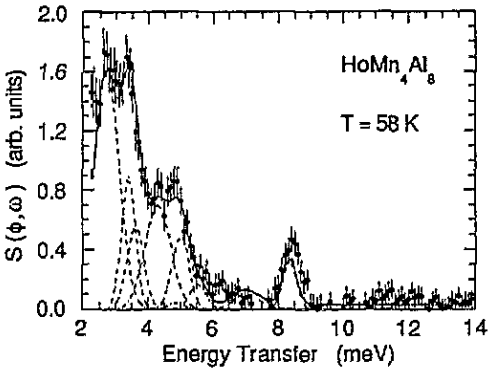

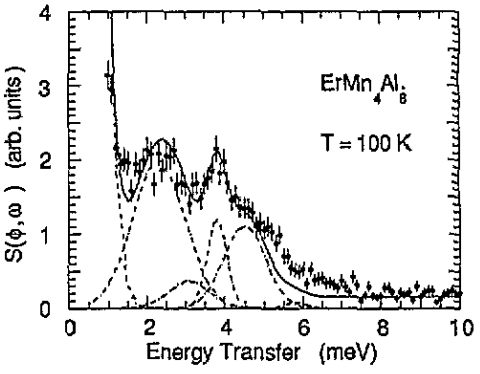

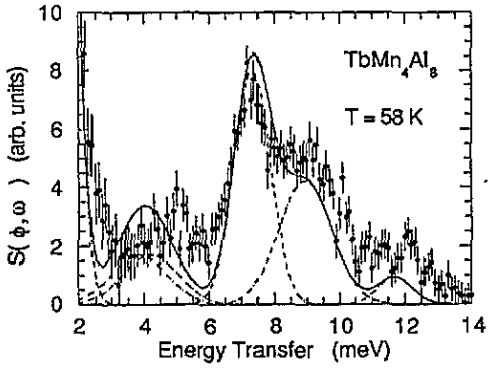

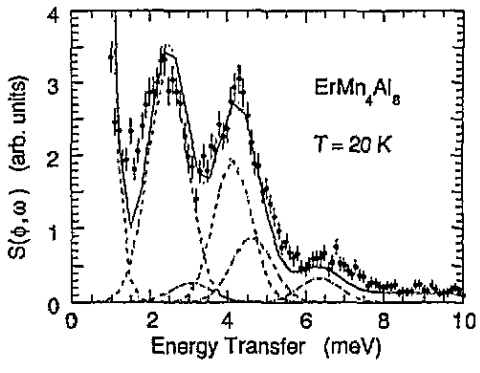

Figure 2. The magnetic neutron scattering response at a temperature $T = 58$ K measured as a function of the energy transfer $\hbar\omega$ for $TbMn_4Al_8$ and $HoMn_4Al_8$. The full line is the spectrum calculated from the model CF Hamiltonian, as described in the text. Individual excitations are indicated by broken lines.

Figure 3. The small-angle ($\phi = 5°$) INS spectrum for $ErMn_4Al_8$ at (a) $T = 20$ K and (b) $T = 100$ K. The calculations use the best-fit CF parameters given in table 2 as shown by the full line. The broken lines represent the individual excitations contributing to the spectra.

varies from 2.85 Å^{-1}, at $\hbar\omega = 2$ meV, to 3.87 Å^{-1}, at $\hbar\omega = 12$ meV. No peaks are observable in the same energy transfer region for YMn_4Al_8, the cross section of which is essentially flat, ruling out the possibility that the excitations arise from vibrational scattering.

Figure 3 shows the results obtained for $ErMn_4Al_8$ at $T = 20$ K and $T = 100$ K, with a full scattering angle $\phi = 5°$. Measurements at larger scattering angles, up to $\phi = 136°$, show a progressive decrease in the peak intensity as Q becomes larger, confirming the magnetic origin of the observed excitations. This is also supported by comparison with the YMn_4Al_8 spectrum at the same temperatures.

The scattering functions obtained for $ErCu_4Al_8$ at $T = 50$ and 100 K with full scattering angle $\phi = 10°$ are shown in figure 4, whereas figure 5 shows the results obtained with the same instrumental configuration for $ErFe_4Al_8$, in the paramagnetic phase at $T = 150$ K. The intensity reduction observed as the scattering angle increases, up to $\phi = 74°$, supports the interpretation of the peaks in the neutron cross section as magnetic excitations.

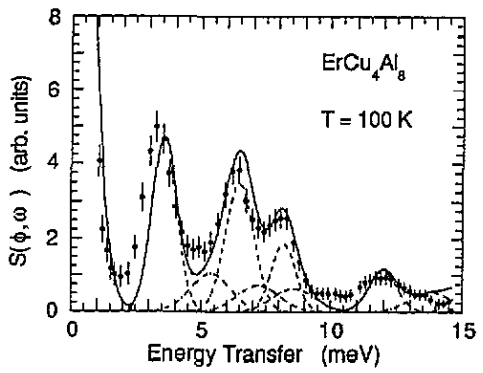

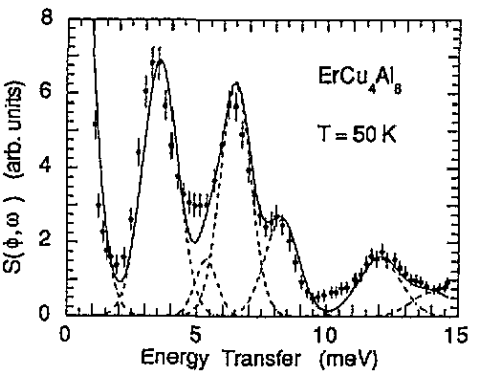

Figure 4. Background-corrected magnetic excitation spectra obtained for $ErCu_4Al_8$ at (a) $T = 50$ K and (b) at $T = 100$ K, with full scattering angle $\phi = 10°$. The full line is the fit to the data with the CF parameters reported in table 2.

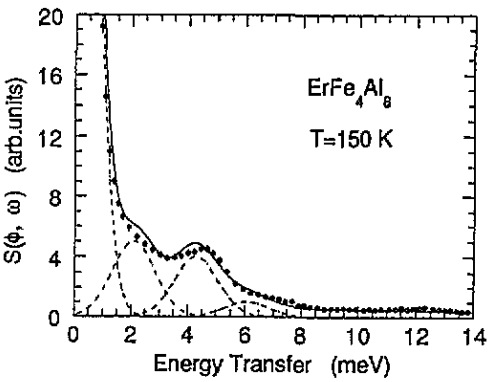

Figure 5. Background-corrected magnetic neutron scattering spectrum obtained for $ErFe_4Al_8$, in the paramagnetic phase at $T = 150$ K. Full scattering angle $\phi = 10°$. The full line is the fit to the data with the CF parameters reported in table 2.

3. Data analysis

The magnetic scattering function $S(Q, \hbar\omega)$ for unpolarized neutrons in the dipole approximation for a system of N non-interaction ions can be written as [15]

$$S(Q,\hbar\omega) = \frac{N}{4}(g_N r_e)^2 f^2(Q) g_J^2 \sum_{i,f} p_i |\langle f|J_\perp|i\rangle|^2 P(\hbar\omega - \Delta_{fi}, \Gamma_{fi}) \qquad (1)$$

where $(g_N r_e)^2 = 0.29$ b sr^{-1}, $|n\rangle$ are the 4f-electron eigenstates with energies E_n and thermal occupation probabilities p_n, $J_\perp$ is the total angular momentum component perpendicular to the scattering vector and $P(\hbar\omega - \Delta_{fi}, \Gamma_{fi})$ is the lineshape for a peak of full width at half-maximum Γ_{fi} and energy transfer centred at $\Delta_{fi} = E_f - E_i$.

The matrix elements and the energies can be obtained by diagonalization of the CF Hamiltonian which, for the RE ion in tetragonal symmetry and the z axis as the quantization axis, is

$$H_{CF} = B_2^0 \hat{O}_2^0 + B_4^0 \hat{O}_4^0 + B_4^4 \hat{O}_4^4 + B_6^0 \hat{O}_6^0 + B_6^4 \hat{O}_6^4 \qquad (2)$$

where the $B_n^m = A_n^m \langle r^n \rangle \theta_n$ are the CF parameters, $\theta_n = \alpha_J$, β_J, γ_J are the Stevens coefficients, $\langle r^n \rangle$ are the moments of the 4f radial wavefunction and the $\hat{O}_n^m$ are the Stevens

operator equivalents built up of the total angular momentum operators [16]. The degeneracy of the $^7F_6$ Russell–Saunders ground-state multiplet of the Tb^{3+} ions is partly lifted by the CF into three Kramers doublets and seven singlets, whilst the $^5I_8$ Ho^{3+} ground state is split into four doublets and nine singlets. The Er^{3+} Russell–Saunders ground state is $^4I_{15/2}$, and it is split by the CF into eight Kramers doublets.

The peaks in the INS cross section correspond to dipole-allowed magnetic transitions between the CF levels. Their energy gives a direct measurement of the eigenvalues of the CF Hamiltonian, and their intensities provide information about the CF wavefunctions through the matrix elements of $J_\perp$. In principle, at least one set of the Hamiltonian parameters B_n^m can be determined from the experimental data by a least-squares fit procedure, but a good starting set of parameters is needed in order to obtain a solution with a physical meaning, and not just a minimum in a numerical problem. In a purely ionic system, a reasonable starting set may be provided by a point-charge model (PCM) calculation. However, for intermetallic systems such as RET_4Al_8, the attribution of an effective ion charge to each ion in the crystal, with the only constraint of electric neutrality, is quite arbitrary, and PCM results are usually unreliable. On the contrary, a realistic estimate of the size and sign of the ratios B_4^0/B_4^4 and B_6^0/B_6^4 could be obtained by exploiting the Newman superposition model (SM), which assumes that the CF is the superposition of two-body potentials due to the nearest-neighbour ions alone [17]. In this way, by fixing the ratios between the fourth-order and sixth-order terms to the SM calculations, it is possible to reduce to three the number of independent parameters to be determined by the least-squares fit.

In a first attempt to interpret our experimental data, we followed this approach. Although we failed to find a unifying picture for the RET_4Al_8 series, it appeared that the second-order term in the CF Hamiltonian was the most important in determining the characteristics of the spectrum. On the other hand, experimental information on B_2^0 can be obtained from the Mössbauer spectroscopy data for $^{155}GdT_4Al_8$ (T = Cu, Fe or Mn) which are available from the literature [6]. In fact, the lowest-order CF term B_2^0 can be factorized as the product of a factor which depends on the shape and the radial distribution of the electron cloud around the nucleus, and a parameter A_2^0 which is independent of the RE ion, being $B_2^0 = \alpha_J \langle r^2 \rangle A_2^0$. The A_2^0 parameter is, in turn, related to the measured nuclear quadrupole splitting through the equation [18]

$$A_2^0 = -2021 \frac{e^2qQ}{Q(1-\gamma_\infty)} (\mathrm{meV} a_0^{-2}) \tag{3}$$

where the quadrupole coupling constant e^2qQ is given in millimetres per second and the quadrupole moment of the nucleus Q is given in barns. In equation (3), a_0 is the Bohr radius, eq is the field gradient and γ_∞ is the Sternheimer antishielding factor. For ^{155}Gd it is $Q(1-\gamma_\infty) = 121$ b [19]. The values $e^2qQ = -1.182$ mm s^{-1}, $e^2qQ = -3.425$ mm s^{-1} and $e^2qQ = 3.123$ mm s^{-1} have been reported for GdT_4Al_8 with T = Cu, Fe and Mn, respectively [6].

Recent band-structure calculations have shown that equation (3) has no sound physical basis [20]. In fact, it is the 5d electron asphericity which mainly contributes to A_2^0, whereas it is the generally different 6p-electrons asphericity which determines e^2qQ. Nevertheless, there are strong indications that an empirical relation between A_2^0 and e^2qQ still exists. For instance, the changes in the sign and magnitude of A_2^0 found by means of single-crystal magnetization measurements and INS experiments in the series $REGd_{2-x}Al_x$ could be accurately followed (within 3%) by a similar behaviour of e^2qQ determined from Gd Mössbauer spectroscopy on the corresponding Gd compounds [21]. It should be noted that the relation given in the previous reference, namely $A_2^0 = -6.8e^2qQ$, leads to an A_2^0

value smaller than that obtained by equation (3). The disagreement is only apparent, since equation (3) gives the 'bare' A_2^0, which does not include the modification of the CF on the 4f electrons due to the polarization of the outer $5s^25p^2$ electron shells. This effect reduces the second-order CF parameters by a shielding factor $1-\sigma_2$, with $\sigma_2 \approx 0.6$ for ions of the RE series [22].

Therefore, by means of equation (3), it is possible to estimate A_2^0 for the different compounds investigated in the present work and, subsequently, the values of B_2^0. For $REMn_4Al_8$, taking into account the shielding factor $1-\sigma_2$, one obtains $B_2^0 = 0.17$ meV for RE = Tb^{3+} ions, $B_2^0 = 0.03$ meV for RE = Ho^{3+}, and $B_2^0 = -0.04$ meV for RE = Er^{3+}. In the case of ErT_4Al_8, one has $B_2^0 = 0.014$ meV for T = Cu and $B_2^0 = 0.04$ meV for T = Fe. The values quoted above have been taken as starting points in a least-squares fitting procedure of the measured profiles based on the diagonalization of the Hamiltonian (2) and on the assumption of Gaussian lineshapes for the individual excitations.

Table 2. Crystal-field parameters for RET_4Al_8 compounds, as obtained from the present experiment. a_0 is the Bohr radius, and $n = 2, 4, 6$.

	$TbMn_4Al_8$	$HoMn_4Al_8$	$ErMn_4Al_8$	$ErCu_4Al_8$	$ErFe_4Al_8$
$10\ B_2^0$ (meV)	0.77(11)	0.28(6)	−0.36(2)	0.20(4)	0.40(4)
$10^4\ B_4^0$ (meV)	4.4(7)	−0.75(7)	1.3(2)	0.2(1)	2.1(2)
$10^5\ B_6^0$ (meV)	0.24(7)	0.23(4)	−0.28(8)	−0.69(2)	−0.27(3)
$10^3\ B_4^4$ (meV)	2.2(9)	−0.11(9)	0.09(17)	−0.3(2)	0.2(1)
$10^5\ B_6^4$ (meV)	0.34(20)	0.34(19)	−0.61(12)	−4.4(5)	−0.6(2)
A_2^0 (meV a_0^{-n})	−9.2(1.4)	−17(3)	−19(1)	11(6)	22(2)
A_4^0 (meV a_0^{-n})	2.4(3)	1.6(1)	2.4(3)	4(2)	37(6)
A_6^0 (meV a_0^{-n})	−0.31(8)	−0.34(6)	−0.27(8)	−0.69(2)	−0.27(3)
A_4^4 (meV a_0^{-n})	11(4)	2.4(1.1)	1.7(3)	−5(2)	4(2)
A_6^4 (meV a_0^{-n})	−2.1(1.2)	−0.49(25)	−0.64(12)	−4.4(5)	−0.6(2)

4. Discussion and conclusions

The B_n^m CF coefficients leading to the best fit of the observed magnetic scattering function for the investigated compounds are reported in table 2, together with the corresponding A_n^m. The calculated profiles are shown as solid lines in figures 2–5, and they appear to be in good agreement with the experimental observations.

In the same environment, different RE ions should experience a similar CF. A test for the physical soundness of a proposed CF model is therefore that the A_n^m parameters should have the same sign and order of magnitude for a series of isostructural RE compounds. As shown in table 2, this appears to be the case for the $REMn_4Al_8$ compounds. An interesting result is the change in sign of the electric field gradient (opposite to the sign of A_2^0) from negative for T = Cu and Fe to positive for T = Mn, which could be attributed to differences in the nearest-neighbour distances and in the charge-density distributions around the transition-metal ions. Because the second-order Stevens coefficient α_J is positive for Er^{3+} (pancake-shaped 4f electronic cloud) but negative for Ho^{3+} and Tb^{3+} (cigar-shaped charge cloud), B_2^0 is positive for all the compounds except $ErMn_4Al_8$.

Once the CF parameters are known, it is possible to estimate the rare-earth contribution to the magnetic anisotropy constants. In the strong exchange limit at $T = 0$ K, these are

given by [23]

$$K_1 = -\tfrac{3}{2}B_2^0\langle\hat{O}_2^0\rangle - 5B_4^0\langle\hat{O}_4^0\rangle - \tfrac{21}{2}B_6^0\langle\hat{O}_6^0\rangle$$
$$K_2 = \tfrac{35}{8}B_4^0\langle\hat{O}_4^0\rangle + \tfrac{189}{8}B_6^0\langle\hat{O}_6^0\rangle \qquad (4)$$
$$K_2' = \tfrac{1}{8}B_4^4\langle\hat{O}_4^0\rangle + \tfrac{5}{8}B_6^4\langle\hat{O}_6^0\rangle$$

where the expectation values refer to the diagonal matrix elements for the Zeeman ground state, $J_z = -J$. With the parameters reported in table 2, one obtains a negative K_1 for all the samples except $ErMn_4Al_8$. A negative K_1 means that an easy-plane magnetic arrangement is favoured by the RE, in competition with the transition-metal anisotropy which could be either planar or axial. Spin reorientation transitions might be expected, unless the total anisotropy is dominated, whatever the temperature, by the contribution of one of the sublattices. If a spin reorientation occurs, it should be a direct axis-to-plane transition in the case of $HoMn_4Al_8$, for which K_2 is negative, whereas the other compounds, which have a positive K_2, should exhibit an axis-to-cone transition. Moreover, in $TbMn_4Al_8$ and $ErFe_4Al_8$, with a positive K_2', the magnetization direction should rotate at low temperatures from [001] towards [110].

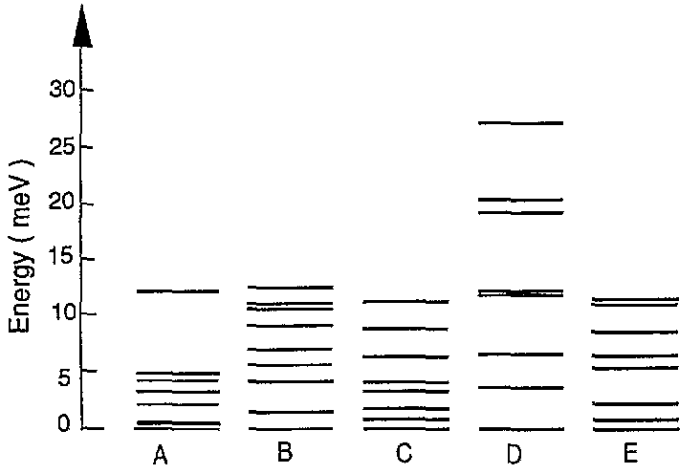

Figure 6. The CF energy level schemes calculated for RET_4Al_8 compounds with the CF parameters reported in table 2. The thick lines represent doublets or closely spaced singlets: A, $TbMn_4Al_8$; B, $HoMn_4Al_8$; C, $ErMn_4Al_8$; D, $ErCu_4Al_8$; E, $ErFe_4Al_8$.

The CF energy level schemes obtained in the present study are shown in figure 6. The ground state of $TbMn_4Al_8$ is a quasi-triplet with a low-lying singlet followed at 0.33 meV by a doublet containing $|J_Z = \pm 5\rangle$, $|J_Z = \pm 3\rangle$ and $|J_Z = \pm 1\rangle$ wavefunctions. In the case of $HoMn_4Al_8$, the ground state is a singlet dominated by the $|J_Z = 0\rangle$ component, the next level being a $|J_Z = \pm 1\rangle$ doublet at 1.3 meV. In the $ErMn_4Al_8$ compound an almost pure $|J_Z = \pm\frac{9}{2}\rangle$ doublet lies at 0.81 meV above the ground state. For all the investigated $REMn_4Al_8$ the total splitting of the fundamental multiplet is close to 12 meV. In $ErFe_4Al_8$ the ground state is a doublet, the next level being an almost pure $|J_Z = \pm\frac{9}{2}\rangle$ doublet lying at only 0.85 meV; the total splitting is about 11 meV. In the case of $ErCu_4Al_8$, the fundamental multiplet is split by 27 meV and the first excited state at 3.6 meV is a doublet dominated by the $|J_Z = \pm\frac{5}{2}\rangle$ wavefunction.

There is some disagreement between the CF parameters determined in this work and the data previously published for the Mn series [13, 14]. The present analysis, however, can be taken to be quite conclusive, especially in the light of the crucial Mössbauer data for $^{155}GdT_4Al_8$.

References

[1] Szytula A and Leciejewicz J 1994 *Handbook of Crystal Structures and Magnetic Properties of Rare-Earth Intermetallics* (Boca Raton, FL: CRC Press)
[2] Buschow K H J 1988 *J. Appl. Phys.* **63** 3130
[3] Kou X C, Zhao T S, Grössinger R, Kirchmayr H R, Li X and de Boer F R 1993 *Phys. Rev.* **47** 3231
[4] Moze O, Caciuffo R, Hong-Shuo Li, Bo-Ping Hu, Coey J M D, Osborn R and Taylor A D 1990 *Phys. Rev.* **42** 1940
[5] Boltich E B, Ma B M, Zhang L Y, Pourarian F, Malik S K, Sankar S G and Wallace W E 1989 *J. Magn. Magn. Mater.* **78** 364
[6] Felner I and Nowik I 1979 *J. Phys. Chem. Solids* **40** 1035; 1978 *J. Phys. Chem. Solids* **39** 951
[7] Felner I and Nowik I 1988 *J. Magn. Magn. Mater.* **74** 31
[8] Florio J V, Rundle R E and Snow A I 1952 *Acta Crystallogr.* **5** 449
[9] Moze O, Ibberson R M, Caciuffo R and Buschow K H J 1990 *J. Less-Common Metals* **166** 329
[10] Shaked H, Pinto M and Felner I 1979 *AIP Conf. Proc.* **53** 295
[11] Gal J *et al* Kalvius G M, Will G and Schäfer 1989 *Phys. Rev.* B **40** 745
[12] Gal J *et al* Pereda J A, Kalvius G M, Litterst F J, Schäfer W and Will G 1990 *Phys. Rev.* B **42** 8507
[13] Moze O, Buschow K H J, Osborn R, Bowden Z and Taylor A D 1989 *Solid State Commun.* **72** 248
[14] Moze O, Caciuffo R and Buschow K H J 1990 *Solid State Commun.* **76** 331
[15] Birgeneau 1972 *J. Phys. Chem. Solids* **33** 59
[16] Hutchings M T 1964 *Solid State Phys.* **16** 227
[17] Newman D J and Ng B 1989 *Rep. Prog. Phys.* **52** 699
[18] Ofer S, Nowik I and Cohen S G 1968 *Chemical Applications of Mössbauer Spectroscopy* ed V J Goldanskii and R H Herber (New York: Academic) p 427
[19] Czjzek G, Oestreich V, Schmidt H, Latka K and Tomala K 1989 *J. Magn. Magn. Mater.* **79** 42
[20] Coehoorn R, Buschow K H J, Dirken M W and Thiel R C 1990 *Phys. Rev.* B **42** 4645
[21] Mulder F M, Thiel R C and Buschow K H J 1994 *J. Alloys Compound.* **203** 97
[22] Sternheimer R M, Blume M and Peierls R F 1968 *Phys. Rev.* **173** 376
[23] Rudowicz C 1985 *J. Phys. C: Solid State Phys.* **18** 1415